DOE/ET-53088-612 IFSR #612

Transport in the Self-Organized Relaxed State of Ion Temperature Gradient Instability

T. TAJIMA, Y. KISHIMOTO,[a] M.J. LEBRUN, M.G. GRAY,
J-Y. KIM, W. HORTON, V. WONG,
and M. KOTSCHENREUTHER
Institute for Fusion Studies
The University of Texas at Austin
Austin, Texas 78712

June 1993

[a] *Naka Fusion Research Estab., JAERI, Naka, Japan*

Transport in the Self-Organized Relaxed State of Ion Temperature Gradient Instability

T. Tajima, Y. Kishimoto,[a] M.J. LeBrun, M.G. Gray, J-Y. Kim,
W. Horton, V. Wong, and M. Kotschenreuther
Institute for Fusion Studies
The University of Texas at Austin
Austin, Texas 78712

Abstract

We investigate the anomalous heat conduction in a tokamak plasma analytically and computationally. Our toroidal particle simulation shows a new emerging physical picture that the toroidal plasma exhibits marked properties distinct from a cylindrical plasma: (i) the development of radially extended potential streamers localized to the outside of the torus, (ii) more robust ion temperature gradient instability, (iii) radially constant eigenfrequency, (iv) global temperature relaxation, and (v) radially increasing heat conductivity χ_i. These results are analyzed by linear and quasilinear kinetic theory. A relaxation theory based on the reductive perturbation theory in the quasilinear equation is developed. The theory constrains the thermal flux so that χ_i increases radially. The Bohm-like scaling is found in connection with the radially extended mode structure.

[a] Naka Fusion Research Establishment, JAERI, Naka, Japan

I Introduction

The η_i instability[1] as well as the ion temperature gradient (ITG) instability[2] are possible candidates to explain the anomalous ion thermal transport observed in many large tokamak plasma.[3, 4, 5, 6] In the previous reports[7, 8] we have found that the properties of the η_i and ITG instabilities in a slab (or cylindrical) plasma and those in a toroidal (tokamak) plasma are quite distinct. Simulation runs of the toroidal plasma have shown that the main differences of toroidal modes as compared with cylindrical cases are: (i) the eigenmodes are elongated in the radial direction and nearly global, while cylindrical ones are localized around the rational surfaces; (ii) the toroidal modes have higher growth rates than the cylindrical counterparts; (iii) the eigenfrequencies are nearly constant over an extended radial region; (iv) a global temperature relaxation and enhanced thermal conduction are observed; (v) in particular, the heat conductivity χ_i is an increasing function of the minor radius as opposed to a decreasing one in a cylindrical counterpart. These signatures are quite striking, as they are all in the right direction to match more closely with experimental tendencies than the cylindrical characteristics. Thus the importance of the toroidal geometric effects on the physics of these modes and associated transport should be emphasized. These differences are primarily due to the toroidicity-induced coupling of rational surfaces over many poloidal mode numbers.

In the present article we shall characterize the temporal evolution of toroidal plasma and the η_i and ITG modes and the resultant properties of the modes and transport. We study this problem through toroidal particle simulation and linear and nonlinear analysis.

II Toroidal Particle Simulation

Employing the Toroidal Particle Code,[9] we investigate the η_i and ITG instability in a toroidal plasma, simulating a tokamak plasma. In the present investigation we use the fully dynamic

ions with adiabatic electrons with the following typical parameters: the aspect ratio $R_0/a = 4$, the average ratio of the ion plasma frequency to ion cyclotron frequency $\langle \omega_{pi}/\omega_{ci} \rangle = 1$, the average ratio of the ion Larmor radius to minor radius $\langle \rho_i/a \rangle \approx 0.02$, the magnetic shear parameter $\hat{s} = rq'/q \sim 1.0$, the Debye length $\lambda_{Di} \approx \rho_i$, and the toroidal mode number(s) $n = 9$; 7 and 9; 7, 9, and 16; 7, 8, and 9, while the poloidal mode numbers vary from $m = 4$ to 39. The profiles of the safety factor $q(r)$, $\hat{s}(r)$, $\rho_i(r)$, and the density scale length parameter $\epsilon_n(r)$ are identical or similar to those shown in Fig. 5 of Ref. 7. For the η_i mode runs, we choose the initial η_i parameter $\eta_i(r) \equiv \partial \ell n\, T_i(r)/\partial \ell n\, n_i(r) =$ constant, varying from 0 to 4 with $n_i(r)$ being a Gaussian. For the ITG ($\eta_i \rightarrow \infty$) mode runs, we choose the parameter $\epsilon_T \equiv L_T/R$ (where L_T is the ion temperature gradient length and R the major radius) typically ranging around 0.07. In this case the initial temperature profile may be a Gaussian or $\tan^{-1}$ profile.

Typical temperature relaxation in time is shown in Fig. 1(a) for the ITG modes. A radial portion of an exponential shoulder ($T_i(r) \propto e^{-r/L_T}$) shows up in a rapid time scale (in a time comparable to the wave growth). The extent of that portion (with the exponential profile) gradually expands until almost all radial portions that encompass the rational surfaces. For the η_i modes the radial profile relaxes from $\tan^{-1}$ towards that of the Gaussian, for which the initial $\eta_i(r; t = 0)$ changes (overall decreases) to become a global constant $\eta_i(t_0)$. This is shown in Fig. 2(a). During these relaxations (either for ITG or for η_i modes) the respective parameter ϵ_T or η_i that characterizes the instability tends to become a global constant. Once these self-similar (or universal) profiles are achieved, the system evolves much more slowly with the profile functional form kept intact (this may be called the profile consistency[10]) but the value of ϵ_T^{-1} or η_i gradually decreasing toward the marginal stability value. This trend is shown in Fig. 1(c) for ϵ_T and in Fig. 2(b) for η_i respectively. Corresponding to the globally (nearly) constant ϵ_T (or η_i), the (nearly) globally constant eigenfrequency appears as shown in Fig. 1(b). Our observation of the global eigenvalue and eigenfunction is consistent with

2D linear theory results.[11] The step-like feature in Fig. 1(b) is due to another eigenvalue. Following the change of global constant ϵ_T, the eigenfrequency also changes accordingly, as shown in Fig. 1(d).

The ion heat conductivity χ_i for the value $\eta_i = 4$ at the end of runs is plotted as a function of the minor radius in Fig. 3 (with single n runs as well as multiple n's). In all cases the χ_i is an increasing function of r (nearly exponential). As noted in Ref. 7 this is a salient feature of toroidal plasma in contrast to that of cylindrical case in which χ_i decreases as a function of r. The latter would be the case if the heat diffusivity is determined by a local diffusion step Δr that is tied to the local temperature (and thus the local Larmor radius). On the other hand, the appearance of the radially increasing χ_i indicates some mechanism that is global in nature. This indication coincides with the implications of the toroidal mode characteristics we describe in the above. Furthermore, in many large tokamak high temperature discharges produced by auxiliary heating such radially increasing χ_i behaviors are universally reported.[3, 4, 5, 6]

In Fig. 4 we show typical temporal evolution of the amplitude of electric potential ($m = 9, n = 9$) and three snapshots of potential contours in r and θ, corresponding to the three stages marked by I, II, and III. Stage I is the linear state, II around the saturation (early nonlinear), and III in the steady state (fully developed nonlinear). The radially extended nearly global mode structure is evident throughout those three stages, including the latest steady nonlinear stage. The potential vortices are strongly twisted and choppier away from $\theta = 0$ (torus outside), while near $\theta = 0$ the prominent ballooning structure is evident.

III Linear and Quasilinear Theory

As we described above, the temperature gradient decreases toward a marginal stable value. In the TPC simulation even in the stage when the mode amplitude is saturated, the temperature profile appears to be slightly on the unstable side so that there occurs constant excitation of

waves whose energy is expended on the transport maintaining a level of heat flux. In order to theoretically describe the toroidal ITG modes, we calculate the perturbed circulating nonadiabatic ion distribution $\widehat{f}_i^{na} = \widehat{g}\,\exp(i\mathcal{L})$ in the ballooning space at $\theta = 0$ as

$$\widehat{g} = \frac{e\widehat{\phi}}{T_i}\,J_0(u)\,\frac{\Omega - \Omega_{*i}^T\left(\widetilde{v}_\parallel^2 + \widetilde{v}_\perp^2 + \eta_i^{-1} - 3/2\right)}{\Omega - (\widetilde{v}_\parallel^2 + \widetilde{v}_\perp^2/2) - \Omega_t\,\widetilde{v}_\parallel}\,f_M\ , \tag{1}$$

and $\mathcal{L} = \mathbf{v}\times\mathbf{b}\cdot\mathbf{k}_\perp/\omega_{ci}$ ($\mathbf{b}\equiv\mathbf{B}/B$) for $\mathrm{Im}\,\omega > 0$. In Eq. (1), f_M represents the local Maxwellian, and $\Omega = \omega/\omega_d$, $\Omega_{*i}^T = \omega_{*i}^T/\omega_d$, $\Omega_t = k_\parallel v_i/\omega_d$, $u = k_\theta\,\rho_i\,\widetilde{v}_\perp$, $\widetilde{v}_\parallel = v_\parallel/v_i$, and $\widetilde{v}_\perp = v_\perp/v_i$ ($v_i \equiv (2T_i/M_i)^{1/2}$) where $\omega_{*i}^T = -(cT_i/eB)(k_\theta/L_T)$, and $\omega_d = 2\epsilon_T\omega_{*i}^T$ is magnetic drift frequency. When the mode approaches the marginal stability, the denominator in Eq. (1) also approaches zero, giving rise to kinetic resonant effects. This underlines the importance of kinetic effects in the present problem. Using Eq. (1), the linear theoretical dispersion relation was derived and the real and imaginary parts of eigenfrequency were computed. The result[12] shows that as the ϵ_T increases and approaches the marginal stability ϵ_{Tc}, that is, when the growth rate γ decreases toward zero, the real frequency of the eigenvalue first rapidly decreases toward a value roughly ω_d (the magnetic drift frequency) and then tends to be a constant (of order unity) times ω_d. As far as $k_\parallel v_i/\omega_d \ll 1$, the real frequency ω_r approaches a constant $\omega_r \sim \omega_d$, where the growth rate γ is around a fraction of ω_d, where the fraction is estimated about $\frac{1}{4}$.

The evolution of the background distribution function f_0 may be described by a quasi-linear theory: $\partial f_0/\partial t = \mathcal{L}[E(\widehat{f}), \widehat{f}]$, where $\widehat{f}$ is the perturbed distribution, E the electric field generated by $\widehat{f}$, and $\mathcal{L}$ is the usual Vlasov operator. When we make a second moment of velocity of this quasilinear equation, we obtain an equation describing the background temperature evolution:

$$\frac{3}{2}\,n\,\frac{\partial T}{\partial t} + \boldsymbol{\nabla}\cdot\mathbf{Q} = 0\ , \tag{2}$$

where the source term is neglected (consistent with the simulation situation), T refers to the background temperature and Q is the second moment of velocity of the term $\mathcal{L}[E(\widehat{f}), \widehat{f}]$ and

it takes the form

$$rQ = \mathrm{Re} \int d\mathbf{v} \frac{1}{2} m v^2 \frac{c\mathbf{E}^* \times \mathbf{B} \cdot \hat{\mathbf{e}}_r}{B^2} \cdot g \exp(i\mathcal{L}) \ ,$$

$$= \frac{n_0 \, r \, k_\theta c e}{B} |\phi(r)|^2 G(\Omega, \eta_i, L_T, r) \ , \tag{3}$$

where Q has the meaning of heat flux due to the fluctuating electric fields E and G is the normalized heat flux (of the order unity). From Eq. (1) G is given as

$$G = -\frac{i}{\sqrt{\pi}} \int_0^{+\infty} dv_\perp^2 \int_{-\infty}^{+\infty} dv_\parallel \, J_0^2(u)(\tilde{v}_\parallel^2 + \tilde{v}_\perp^2) \frac{\Omega - \Omega_{*i}^T(\tilde{v}_\parallel^2 + \tilde{v}_\perp^2 + \eta_i^{-1} - 3/2)}{\Omega - (\tilde{v}_\parallel^2 + \tilde{v}_\perp^2/2) - \Omega_t \, \tilde{v}_\parallel}$$

$$\cdot \exp(-\tilde{v}_\parallel^2 - \tilde{v}_\perp^2) \tag{4}$$

for $\mathrm{Im}\ \omega > 0$. For the stable region the velocity integrals must be carried out with analytical continuation from $\mathrm{Im}\ \omega > 0$ to $\mathrm{Im}\ \omega < 0$ across the marginal stability. Then, the resonant residual part of G is calculated as

$$G = 4\sqrt{\pi}\,\alpha \left(\Omega + \frac{\Omega_t^2}{4}\right)^{1/2} \int_{-1}^{+1} dy \int_C dt \, J_0^2(u)(\bar{v}_\parallel^2 + 2t) \exp(-\bar{v}_\parallel^2 - 2t)$$

$$\cdot \left[\Omega - \Omega_{*i}^T \left(\bar{v}_\parallel^2 + 2at + \eta_i^{-1} - 3/2\right)\right] \cdot \delta \left[t - \left(\Omega + \frac{\Omega_t^2}{4}\right)(1 - y^2)\right] \tag{4'}$$

where $\bar{v}_\parallel = (\Omega + \Omega_t^2/4)^{1/2} \, y - \Omega_t/2$, and $\alpha = 1/2$ for $\mathrm{Im}\ \omega = 0$ and $\alpha = 1$ for $\mathrm{Im}\ \omega < 0$. Here the integration contour C is chosen so that the complex variable t goes around the pole $t = (\Omega + \Omega_t^2/4)(1 - y^2)$.

It should be noted that the heat flux G in Eq. (4) does not vanish even when the mode becomes marginally stable $\mathrm{Im}\ \omega \to 0$ and stays positive in the neighborhood of $\mathrm{Im}\ \omega = 0$. Numerical integrated value of Eq. (4) is given in Ref. 12. This is in sharp contrast to a fluid theoretical calculation of quasilinear heat flux,[13] where $Q = 0$ at marginal stability.

IV Relaxation Theory for Toroidal Plasma

We discussed the relaxation process of the temperature of the toroidal plasma and modes evolution in Sec. II. In the early stage of the simulation before saturation (roughly corre-

sponding to Stage I in Fig. 4) the temperature profile rapidly (in a fluid time scale) relaxes toward an exponential profile (ITG case). In the later stage the temperature profile relaxes slowly, maintaining the functional form, exponential (ITG case), and its parameter ϵ_T only gradually increasing toward the marginal stability, though ϵ_T is still less than ϵ_{Tc}. In this stage the physics is kinetic, as it is near marginal stability. Since there exist these two distinct time scales in relaxation, we introduce a multiple time expansion in our quasilinear equation (2). A systematic expansion may be carried out by the well-known reductive perturbation method,[14] introducing a smallness parameter ε (which will be determined below). We expand the time scales, temperature, and heat flux as follows:

$$\frac{\partial}{\partial t} = \frac{\partial}{\partial t_0} + \varepsilon^2 \frac{\partial}{\partial t_1} + \varepsilon^4 \frac{\partial}{\partial t_2} + \cdots ,$$

$$T = T_0 + \varepsilon T_1 + \cdots ,$$

$$Q = \varepsilon Q_0 + \varepsilon^2 Q_1 + \cdots , \tag{5}$$

where $Q_0 = -\chi_i^0 \nabla T_0$, $Q_1 = -\chi_i^0 \nabla T_1 - \chi_i^1 \nabla T_0$, and T_0 is the global temperature profile, which, as we showed, exhibits a self-similar profile (exponential for ITG, Gaussian for η_i) and is only slowly varying, i.e. $\partial T_0/\partial t_0 = 0$. The present reductive perturbation theory is crucially based on the fundamental properties of relaxation of the tokamak-like toroidal plasma we described. The important point is that the instability is radially global and vigorous in toroidal plasmas so that the plasma parameters have to relax rapidly until they approach sufficiently near the stable profile. (In a cylindrical plasma, therefore, there is no such relaxation theory). However, as long as there is enough heat reservoir (as in our simulation case) or there is energy input, the sustained finite fluctuations will cause a certain amount of heat flux and thus dissipation, which as to be compensated by the weak but still unstable wave activities. The amount of sustained fluctuations thus is a function of the energy (or power) input (or the availability of the heat reservoir).

From this expansion theory we obtain a series of transport equations (as commented on in Eq. (2) we have neglected source terms for clarity of theory. However, it is readily possible to generalize this to include source terms):

$$\mathcal{O}(\varepsilon): \qquad \frac{3}{2} n_0 \frac{\partial T_1}{\partial t_0} + \nabla \cdot Q_0 = 0 \ , \tag{6}$$

$$\mathcal{O}(\varepsilon^2): \qquad \frac{3}{2} n_0 \frac{\partial T_0}{\partial t_1} + \nabla \cdot Q_1 = 0 \ . \tag{7}$$

In Eq. (6) if there is a finite $\nabla \cdot Q_0(r)$, it will force T_1 to rapidly relax such that $T_1 \to 0$. Thus on average we obtain $\partial T_1/\partial t_0 = 0$ and, therefore, $\boldsymbol{\nabla} \cdot \mathbf{Q}_0 = 0$ and

$$r Q_0(r) = r \chi_i^{(0)}(r) \frac{\partial T_0}{\partial r} = \text{const} \ . \tag{8}$$

Thus for ITG in which the relaxed T_0 profile is $\sim \exp(-r/L_T)$ and for η_i the relaxed profile is $T_0 \sim \exp(-r^2/2L_T^2)$, for which the $\mathcal{O}(\varepsilon)$ constraint (8) requires that the thermal conductivity vary as

$$\chi_i^0(\text{ITG}) \sim \frac{\text{const}}{r} \exp(r/L_T) \ , \tag{9}$$

$$\chi_i^0(\eta_i) \sim \frac{\text{const}}{r^2} \exp\left(\frac{r^2}{2L_T^2}\right) \ . \tag{9'}$$

These formulae apply away from the center and edge where the source term effects can never be negligible. These radially increasing χ_i profiles are in agreement with our simulation results, as well as the experimental results.

In the next order in ε, $\mathcal{O}(\varepsilon^2)$, we can obtain the slow evolution of the background temperature $T_0(t_1)$. In the case when $k_\theta \rho_i \ll 1$ (i.e. $J_0^2(u) \sim 1$), and $k_\| \sim 0$, we can write $G(\Omega, L_T, \eta_i, r) = G(\Omega, L_T)$, where Ω and L_T become a global constant due to toroidal plasma properties. Thus

$$r Q(r) = \frac{n_0 \, ce}{B} n \, q(r) |\phi(r)|^2 G(\Omega, L_T) \ , \tag{10}$$

where n is a given toroidal mode number and use is made of $k_\theta^n = nq/r$. Since $rQ(r) = \text{const}$, except for a weak r-dependence of q, Eq. (10) is nearly r-independent, from which we conclude

that $|\phi_0(r)|^2 = |\phi_0|^2 + \varepsilon|\phi_1(r)|^2 + \cdots$, $Q_1(r)$ becomes

$$Q_1 = \frac{n_0\, ce}{B}\, n\, q(r)|\phi_1(r)|^2 G\ . \tag{11}$$

Note that Eq. (6) will not determine the overall strength of Q, although the radial profile is determined. In order to fix the strength of Q or χ_i, we have to employ Eq. (7) as well.

V Heat Conductivity

We investigate the heat conductivity in the presence of ITG (or η_i) driven plasma fluctuations. As we discussed in the previous section, the initial temperature profile evolves rapidly into a self-similar functional form. After this is established, the temperature profile relaxes so that the global parameter (ϵ_T or η_i) slowly change, but the temperature functional form is maintained. After this the profile smoothly tends to the steady-state profile. In this section we try to describe the heat conductivity in each stage. Typically in our initial value simulation the potential fluctuation level shoots up as the linear instability grows until saturation. Then the amplitude tops and later decays or stagnates. The heat conductivity $\chi_i(t)$ evolves in time in a similar fashion; it increases until the saturation time, after which time it decreases and eventually stagnates at a roughly steady value. Using Eq. (10), the ion heat conductivity can be written as

$$\chi_i(r) = \frac{1}{2}\frac{(k_\theta\, \rho_i(r))v_i(r)\, L_T}{T_i(r)^2}\, \left\langle (e\phi(r))^2 \right\rangle\, \mathrm{Re}\ G(\Omega, L_T)\ , \tag{12}$$

where $\left\langle |\phi(r)|^2 \right\rangle$ to the first approximation may be regarded as constant $\langle |\phi_0|^2 \rangle$. It is evident that the equation (12) has a monotonically increasing radial dependence, as given in Eq. (9). In the following we evaluate the heat conductivity in two different regimes, one in the fluid regime and the other in the kinetic one.

A. Hydrodynamic regime

In the present TPC simulation in stages I and II the dynamics is hydrodynamic, while in stage III it is kinetic as discussed in Sec. IV. Hydrodynamic or kinetic is defined by $|\omega + i\gamma| \gtrless \max(k_{\|}\, v_i, \omega_d)$. In this subsection we investigate the heat conductivity in the hydrodynamic regime. However, it is noted that if we had an external power source strong enough, even in the steady saturation stage III we might have the hydrodynamic regime. In this hydrodynamic regime we assume that the saturation mechanism is the wave breaking (i.e. wave turnover effect), since the effect of multiples of the modes (n's) (i.e. the nonlinear mode coupling among different toroidal eigenmodes) is not strong in the present investigations in which the external power source is absent and the heat reservoir is provided only by the central plasma.

The displacement of the plasma fluid by the excited wave k_θ in the radial direction is roughly

$$\xi = \frac{c\, k_\theta \phi}{\gamma_h B} \ , \tag{13}$$

where γ_h is the growth rates in the hydrodynamic regime. When the radial displacement ξ becomes approximately the half wavelength in the radial direction, $\xi \sim \pi/k_r$, the wavebreaking takes place and thus the wave growth saturates. This condition yields the approximate saturated potential amplitude as

$$\phi_{\rm sat} = \frac{\pi\, \gamma_h B}{c\, k_r\, k_\theta} \ . \tag{14}$$

In the hydrodynamic regime the growth rate is estimated to be

$$\gamma_h^2 = \omega_*^T\, \omega_d \ . \tag{15}$$

Thus in the hydrodynamic regime we obtain χ_i from Eq. (12) and approximate expressions (14), (15) as

$$\chi_i^h = 4\pi^2\, \frac{k_\theta\, \rho_i\, v_i\, R\epsilon^2}{(k_r a)^2}\, G_h \ , \tag{16}$$

where $\epsilon = a/R$. The hydrodynamic normalized flux G_h is evaluated as

$$G_h = -\frac{2}{\sqrt{\pi}} i \int_0^\infty dv_\perp \, v_\perp \, J_0^2(u) e^{-v_\perp^2} \int_{-\infty}^\infty dv_\parallel \left[1 + \frac{2}{(2\epsilon_T)^{1/2}} \left(v_\parallel^2 + v_\perp^2 + \frac{1}{\eta_i} - \frac{3}{2} \right) \right]$$

$$\times \left[1 - i\sqrt{2\epsilon_T} \left(v_\parallel^2 + \frac{v_\perp^2}{2} \right) \right] (v_\parallel^2 + v_\perp^2) e^{-v_\parallel^2} \cong \frac{C_1}{\epsilon_T^{1/2}} , \tag{17}$$

where expansion in terms of $1/2\epsilon_T \ll 1$ was carried out and C_1 is a constant of order unity. With Eq. (17), the χ_i expression (16) becomes

$$\chi_i^h = \frac{4\pi^2 \, C_1}{\epsilon_T^{1/2}} \frac{k_\theta \, \rho_i \, v_i \, R\epsilon^2}{(k_r \, a)^2} . \tag{18}$$

Choi and Horton[15] and Romanelli[16] among others have shown that the global linear radial mode width is a geometrical mean of ρ_i and a so that approximately we have

$$(k_r \, a)^2 = \frac{a}{\rho_i} . \tag{19}$$

If the mode width in the nonlinear stage is not too different from the linear stage [this is not inconsistent with our simulation], then Eq. (19) may be used as an estimate in Eq. (18). This yields

$$\chi_i^h = C_2 \left(\frac{cT}{vB} \right) \left(a \, L_T^{-1/2} \, R^{-1/2} \right) , \tag{20}$$

where C_2 is a constant and $\langle k_\theta \, \rho_i \rangle \sim 0.2$ is taken. In our simulation the radial size of the streamer (the potential vortex structure) is about the same as in the linear stage (Fig. 4). In the simulation in particular the ratio $\rho_i/a \sim 1/40$ is approximately eight times larger than the typical experimental value of $\sim 1/300$. This makes the radial size scaling in our simulation about three times greater in terms of the fraction of the minor radius. In the future smaller ratios ρ_i/a will be used at in simulation to definitely resolve the scaling. If we take scalings for the radial streamer size as $k_r^{(s)} \sim 1/\rho_i$ and $k_r^{(\ell)} \sim 1/a$, the corresponding χ_i scalings would be

$$\chi_i^{h(s)} \sim C_2' \left(\frac{cT}{eB} \right) \left(\rho_i \, L_T^{-1/2} \, R^{-1/2} \right) = \sqrt{2} \, C_2' \left(\frac{M^{1/2} \, c^2 \, T^{3/2}}{e^2 \, B^2} \right) \left(L_T^{-1/2} \, R^{-1/2} \right)$$

[corresponding to the gyroBohm scaling] and

$$\chi_i^{h(\ell)} \sim C_2''(v_i\, a)\left(a\, L_T^{-1/2}\, R^{-1/2}\right) ,$$

[corresponding to the hydrodynamic transport scaling] respectively. The ion energy confinement time from Eq. (20) is approximately obtained from $\tau_i^h \sim L_T^2/\chi_i^h$ as

$$\tau_i^h = C_3 \frac{eB}{cT}\, a^{-1}\, L_T^{5/2}\, R^{1/2} , \tag{21}$$

where C_3 is a constant.

B. Kinetic regime

We find in stage III in our simulation that the system reaches close to marginal stability (though slightly above the marginal). This implies that the dynamics is kinetic in this stage. From a closer scrutiny of stage III, we see that the mode amplitude of various waves increases or decreases incessantly as shown in Fig. 4(a). Sometimes a sudden crash of amplitude appears, which usually coincides with reconnection of one vortex occupying radial interval $r \in [r_1, r_2]$ with another at $r \in [r_2, r_3]$. Some resurgence and decay of the mode amplitude are related to a local temperature bump or hole. Detailed description of these processes will be reported elsewhere in the future. The overall behavior of the temperature profile and wave activities is as follows: if there appears a local temperature bump steeper than the global gradient characterized by ϵ_T, the wave activity in the neighborhood is elevated so that the locally enhanced heat conduction will smooth the bump. On the other hand, if there appears a local hole less steep than the global gradient, the wave activity in the vicinity is depressed so that the locally reduced heat conduction is overwhelmed by the overall global rate of heat conduction, which leads to smoothing of the hole. Thus the overall growth rate γ is sustained around a constant γ_c (critical growth rate), which is above the marginal value of zero in order to sustain the overall global energy dissipation (heat transport). The smallness parameter ε is determined as $\sqrt{\gamma_c/\omega_r}$. If γ was less than γ_c, all wave activity would have diminished

and no global heat conduction would be maintained. The heat reservoir provides heat and then lets the temperature profile steepen, which lends to an increase in γ to approach γ_c, where the critical parameter γ_c is much smaller than γ_h or the real frequency ω_r. We call this behavior of the tokamak plasma the self-organized criticality. This is not unlike the situation discussed on the avalanche of a sand pile by Bak *et al.*[17] However, their theory does not have distinction between the marginal stability and critical threshold as ours does, nor do they provide a self-consistent analytic expression for transport. In order to explain the profile consistency, others have resorted to the plasma's self-organizing tendency.[10, 17]

We now wish to derive the ion heat conductivity in the self-organized critical state by evaluating the residual part (4), though there is non-residual contribution. In the kinetic regime, we can approximate $\Omega = 1$ and $\Omega_t = 0$ to estimate the normalized flux G as

$$G_k(\Omega = 1) = \int_{-1}^{1} dx \, \exp(-2 + x^2)(2 - x^2) \left[1 - \Omega_{*i}^T \left(2 - x^2 - \frac{3}{2}\right)\right] \approx C_4 + C_5 \, \Omega_{*i}^T \, , \quad (22)$$

where $\Omega_* = \frac{1}{2\epsilon_T}$ and C_4, C_5 are constants of order unity. The excited waves can scatter particles in this regime to balance the wave growth[19]

$$\gamma - k_r^2 \, D = 0 \, , \quad (23)$$

where the diffusion coefficient due to wave-particle interaction is estimated as

$$D = \frac{\delta \xi^2}{\delta t} = \frac{c^2 k_\theta^2 |\phi|^2}{\delta t \, \omega^2 \, B^2} \, , \quad (24)$$

and

$$\delta t \sim \frac{\pi a}{2 \omega_d \, \hat{s} \, \Delta r} \propto \frac{1}{\omega_d} \quad (25)$$

where Δr is typical radial extension of global eigenmode and δt is estimated from the typical time scale that the global eigenmode is affected by the strong sheared phase rotation in the poloidal direction. Equations (23), (24), and (25) give

$$|\phi|^2 = \frac{B^2 \, \gamma \omega}{(k_\theta \, k_r)^2 c^2} \, . \quad (26)$$

As remarked in Sec. II, when the system approaches from the hydrodynamic regime toward the kinetic one, the growth rate decreases accompanied by a rapid decrease of ω_r first followed by a near plateau value $\omega_r \sim \omega_d$. If we call the entry to the plateau regime (kinetic) begins when ω_r becomes insensitive to the change of ϵ_T and thus γ, the entrance is evaluated at $\gamma = f\,\omega_d$, and $f \cong 1/4$. Equation (26) with $\gamma = f\,\omega_d$ and Eq. (22) [and taking the second term in (22)] give rise to the ion heat conductivity estimate in the kinetic regime as

$$\chi_i^k = C_6 \left(\frac{cT}{eB}\right) (a\, L_T\, R^{-2}) \,, \tag{27}$$

where once again we took $(k_r\, a)^2 = a/\rho_i$ [Eq. (19)] and C_6 is a constant. If, as before, $k_r^{(s)} \sim 1/\rho_i$ and $k_r^{(\ell)} \sim 1/a$ scalings are taken instead, we obtain the corresponding χ_i scalings as

$$\chi_i^{k(s)} \sim C_6' \left(\frac{cT}{eB}\right) (\rho_i\, L_T\, R^{-2})$$

and

$$\chi_i^{k(\ell)} \sim C_6''(v_i\, a)(a\, L_T\, R^{-2})$$

respectively. Note that in the kinetic regime the choice of $(k_r\, a)^2 \cong a/\rho_i$ should be even better justified, as the system is close to the linear stage. The ion energy confinement time derived from Eq. (27) is

$$\tau_i^k = C_7 \frac{eB}{cT}\, a^{-1}\, L_T\, R^2 \,, \tag{28}$$

where C_7 is a constant. The energy confinement time in Eq. (28) is the so-called Bohm scaling proportional to the toroidal field B.

VI Discussion and Conclusions

A characteristic feature of these simulations is an initial nonlinear phase during which linear wave growth saturates and the temperature profile relaxes comparatively rapidly to a self-similar profile not far from marginal stability. In the later nonlinear phase, the self-similar

profile relaxes more slowly towards marginal stability. The radial size of the potential vortex structure is approximately the same as in the linear stage and we estimate radial correlation lengths to be $\sim (\rho_i\, a)^{1/2}$. The thermal diffusivity χ_i scales as (Eq. (16)):

$$\chi_i \sim \frac{\langle k_\theta\, \rho_i \rangle\, v_i\, a^2}{(k_r^2\, a^2) R}$$

and if we take $\langle k_\theta\, \rho_i \rangle \sim \mathcal{O}(1)$ and $k_r (\rho_i\, a)^{1/2} \sim \mathcal{O}(1)$, $\chi_i \propto \frac{a}{R}\, v_i\, \rho_i$, a Bohm-like scaling.

As stated earlier, our simulations and discussion are limited to no (or weak) power input in the radial region of consideration. Thus the scalings Eqs. (21) and (28) do not have an explicit dependence on the input power P. [The input power P might appear through other parameters, as has been done in Ref. 21]. Also implicit in our calculation is the plasma current I, which appear, for example, in $\hat{s}$ but was in our discussion tucked away in such approximations as $\hat{s} \sim 1$. Furthermore, the average ratio of ion Larmor radius to minor radius is $\left\langle \frac{\rho_i}{a} \right\rangle \sim 0.02$, much larger than typical experimental values. Thus a direct one-to-one comparison with experimental data cannot be made. It is, however, interesting to see in light of Eq. (28) that the experimental confinement time goes like $\tau_E \propto B^{0.9}\, R^{2.3}\, \epsilon^{-0.2}$ in Ref. 21 for example.

Other simulation codes[22] have shown nonlinear states with vortex structures significantly smaller than the radial scale lengths of the linear eigenmode. In these simulations, $\frac{\rho_i}{a} \sim \frac{1}{400}$, the initial temperature and density profiles were not close to marginal stability and were "maintained on the average" by imposing periodic boundary conditions. Global change of $\omega_*(r)$, for example, is not allowed in those models,[22] as the shell thickness is much smaller than a. Linear growth does not saturate by profile relaxation but by the onset of a "non-linear" instability resulting in the "break-up" of the linear eigenmode and the formation of vortex structures with characteristic scale lengths of many ion Larmor radii. When this occurs, the potential amplitudes at saturation of linear growth are not determined by Eq. (14), and Eq. (16) for χ_i is no longer applicable. A limited number of runs with these other

simulation codes suggest that the χ_i scaling tends to be gyroBohm.

It is evident that we need many more simulation runs (particularly those of scaling physics) and more detailed theoretical analysis. Such investigations will tell us how much is model dependent and which scalings of χ_i applies. It is the purpose of the present paper to foster the stimulus to such investigations and to give some insight to processes that might be important to consider.

An earlier paper[23] deals with a view that plasma profiles would remain close to marginal stability.

Acknowledgments

This work was supported by the U.S. Department of Energy contract #DE-FG05-80ET-53088.

References

[1]W. Horton, D-I. Choi, and W.M. Tang, Phys. Fluids **24**, 1077 (1981).

[2]B. Coppi, M.N. Rosenbluth, and R.Z. Sagdeev, Phys. Fluids **10**, 582 (1967).

[3]S.D. Scott, *et al.*, Phys. Fluids B **2**, 1300 (1990).

[4]T. Kurki-Suonio, R.J. Groebner, and K.H. Burrell, Nucl. Fusion **32**, 138 (1992).

[5]B. Balet, *et al.*, Nucl. Fusion **30**, 2034 (1990).

[6]JT-60 TEAM, in *Plasma Physics and Controlled Nuclear Fusion Research, 1990*, Vol. 1, p. 53 (IAEA, Vienna, 1991).

[7]M.J. LeBrun, T. Tajima, M. Gray, G. Furnish, and W. Horton, Phys. Fluids B **5**, 752 (1993).

[8]M. Kotschenreuther, *et al.*, in *Plasma Physics and Controlled Thermonuclear Research* (IAEA, Vienna, 1993), to be published.

[9]M.J. LeBrun and T. Tajima, submitted to J. Comput. Phys.

[10]B. Coppi, Comm. Plas. Phys. Contr. Fus. **5**, 261 (1980).

[11]W.M. Tang and G. Rewoldt, to be published in Phys. Fluids B.

[12]Y. Kishimoto, T. Tajima, M.J. LeBrun, M. Gray, J-Y. Kim, and W. Horton, IFSR#589, submitted to Phys. Rev. Lett. (1993).

[13]F. Romanelli, Phys. FluidsB **1**, 1018 (1989).

[14]H. Washimi and T. Taniuti, Phys. Rev. Lett. **17**, 996 (1966).

[15]D-I. Choi and W. Horton, Phys. Fluids **23**, 356 (1980).

[16]F. Romanelli, in this Proceedings.

[17]P. Bak, C. Tang, and K. Wiesenfeld, Phys. Rev. A. **38**, 364 (1988).

[18]B.B. Kadomtsev, Sov. J. Plasma Phys. **13**, 443 (1987).

[19]T.H. Dupree, Phys. Fluids **11**, 2680 (1968).

[20]J. Christiansen, *et al.*, Nucl. Fusion **32**, 316 (1992).

[21]F.W. Perkins, *et al.*, Phys. Fluids B **5**, 477 (1993).

[22]M. Kotschenreuther and V. Wong (private communication, 1993).

[23]W. Manheimer and J.P. Boris, Comments Plasma Phys. Contr. Fusion **3**, 15 (1977).

Figure Captions

1. Growth rate Im ω/ω_d (a) and real part of the frequency Re ω/ω_d (b) versus ϵ_T for different value of $X = k_{\|}\, v_i/\omega_d$. Figure (c) shows the growth rate $\gamma R/v_i$ (solid line) and normalized heat flux $G = \overline{Q} \cdot B/n_0 mce|\phi|^2$ (dashed line) versus $k_\theta\, \rho_i/\sqrt{2}(\equiv k_\theta\, \overline{\rho}_i)$.

2. Temporal change of the plasma temperature profile as observed in our TPC simulation. (a) The initial arctan profile relaxes toward the gaussian with which η_i becomes a global constant. (b) The evolution of η_i as a function of time and radial position (initially gaussian temperature profile).

3. The measured heat conductivity (in the unit of $\rho_i^2\, c_s/L_n$) vs. the main radius of the toroidal plasma from the TPC simulation. Both single helicity runs as well as multi-helicity runs show similar qualitative tendencies.

4. Temporal evolution of the potential energy and potential structures. (a) The potential energy vs. time for three stages I (linear stage), II (saturation), and III (steady). (b) Potential structure in the poloidal cross-section at stage I, (c) at stage II, (d) at stage III. The toroidal outward direction is to the right.

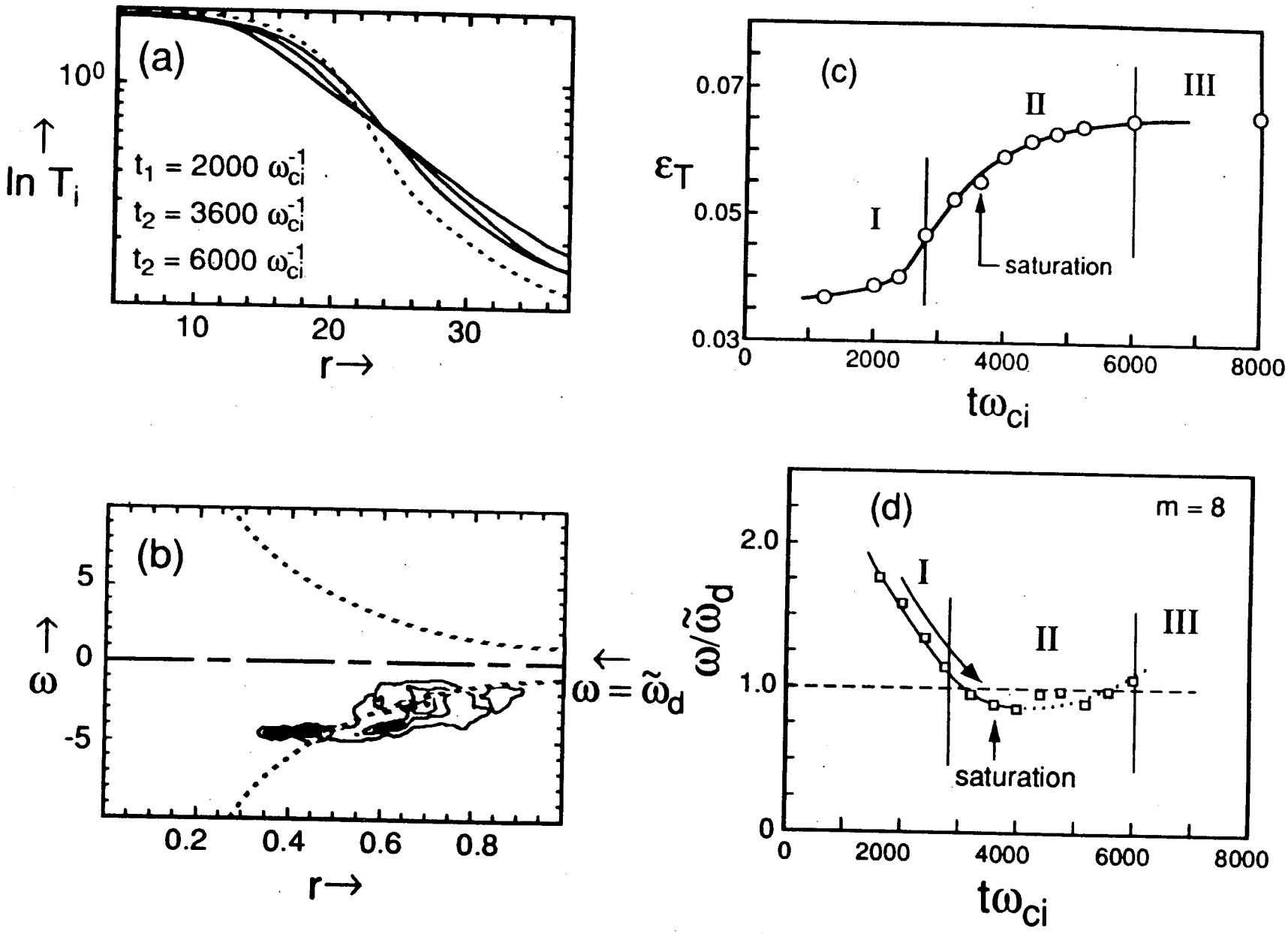
(a)
10^0
ln T_i
$t_1 = 2000\ \omega_{ci}^{-1}$
$t_2 = 3600\ \omega_{ci}^{-1}$
$t_2 = 6000\ \omega_{ci}^{-1}$
10
20
30
r→
(b)
5
0
-5
ω
0.2
0.4
0.6
0.8
r→
$\omega = \tilde{\omega}_d$
(c)
0.07
0.05
0.03
ε_T
I
II
III
saturation
0
2000
4000
6000
8000
$t\omega_{ci}$
(d)
m = 8
2.0
1.0
0
$\omega/\tilde{\omega}_d$
I
II
III
saturation
0
2000
4000
6000
8000
$t\omega_{ci}$

Fig. 1

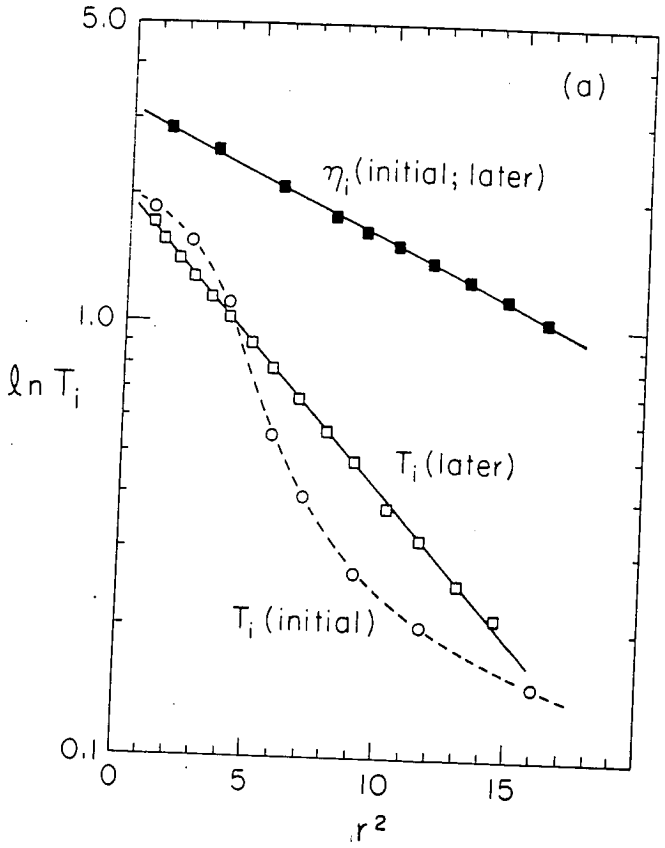
5.0
1.0
0.1
(a)
η_i (initial; later)
T_i (later)
T_i (initial)
ln T_i
0
5
10
15
r^2

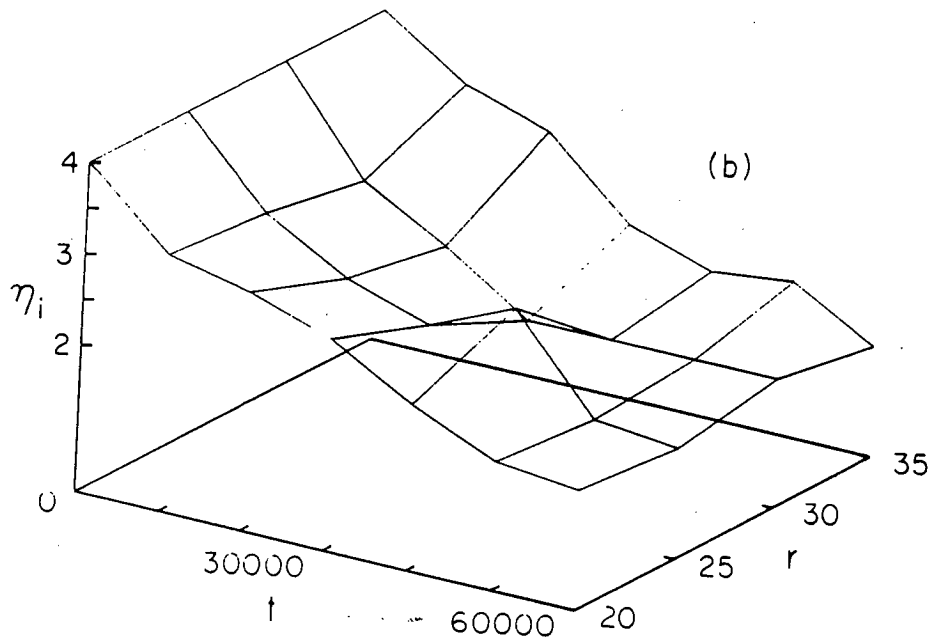
(b)
4
3
2
0
η_i
30000
t
60000
20
25
30
35
r

Fig. 2

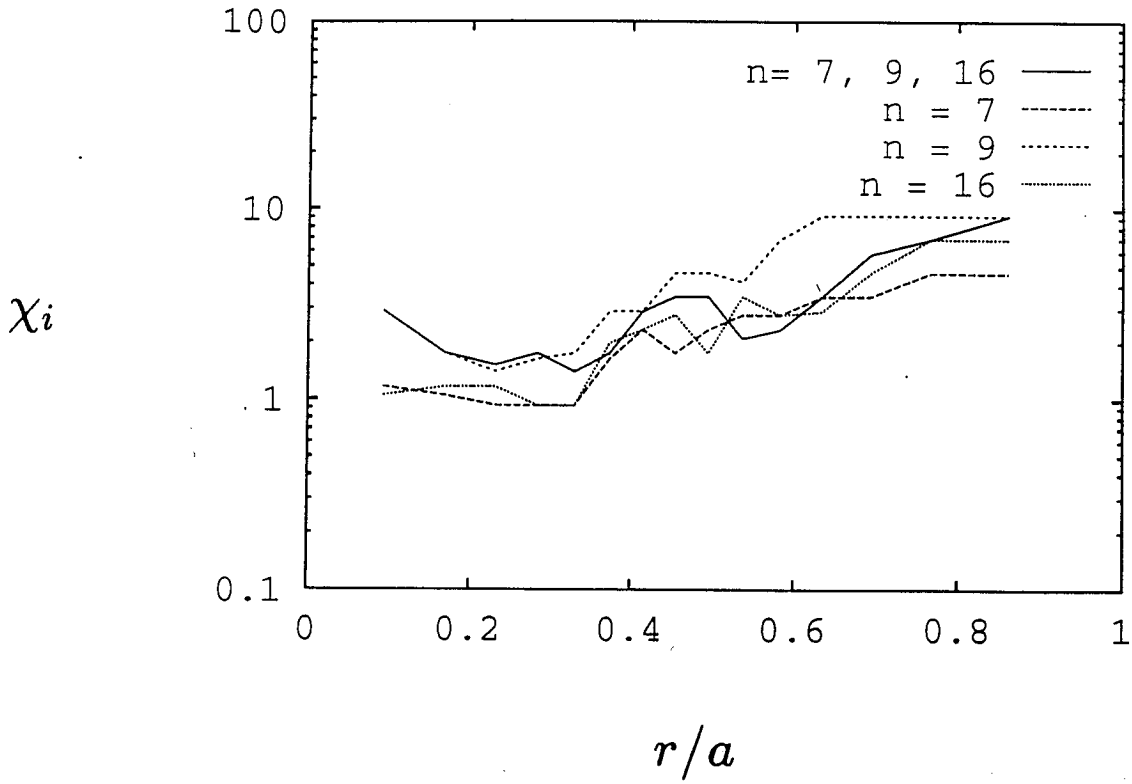

Fig. 3

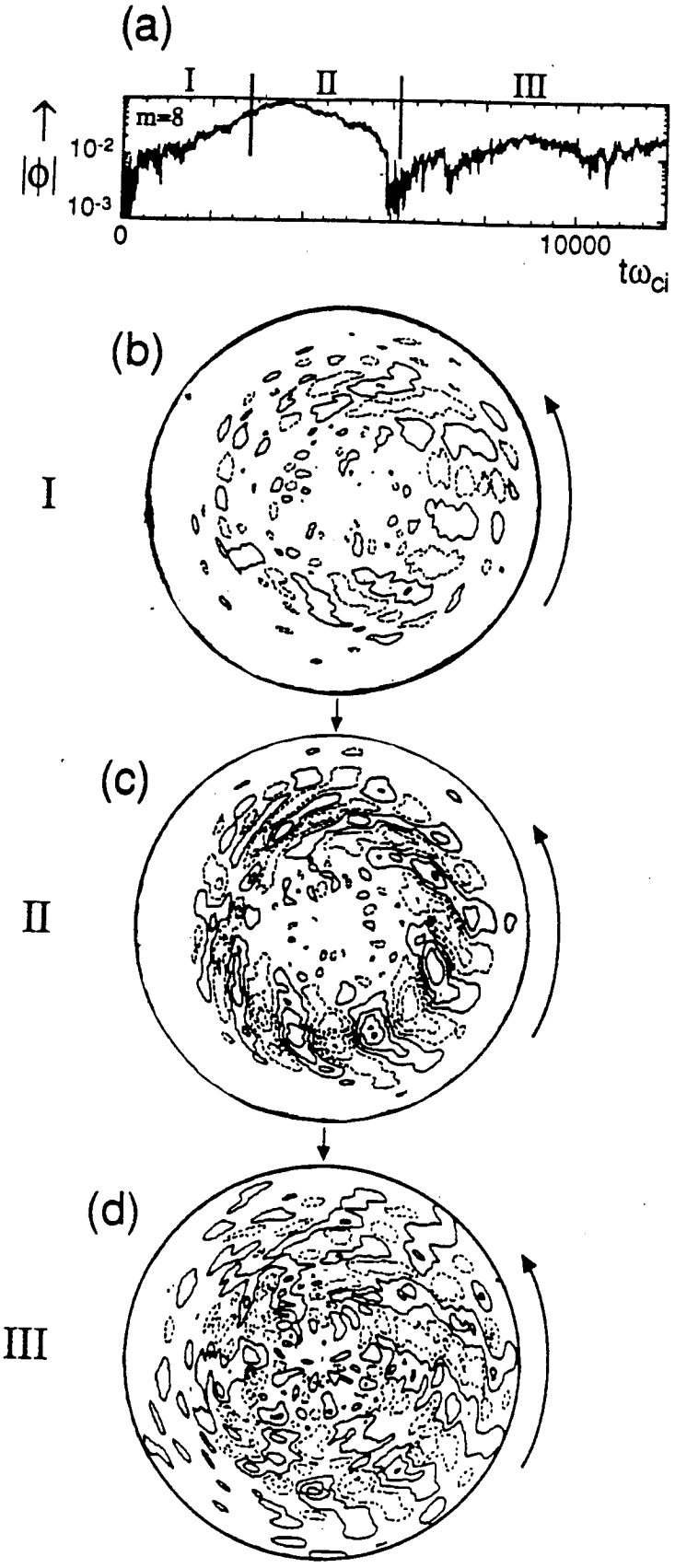

Fig. 4